Available online at www.sciencedirect.com
SCIENCE DIRECT®
PERGAMON
International Journal of Multiphase Flow 29 (2003) 361–373
International Journal of Multiphase Flow
www.elsevier.com/locate/ijmulflow

Experimental study on the interaction between large scale vortices and particles in liquid–solid two-phase flow

Yohsuke Tanaka, Gen Oba, Yoshimichi Hagiwara *

Department of Mechanical and System Engineering, Kyoto Institute of Technology, Goshokaido-cho, Matsugasaki, Sakyou-ku, Kyoto 606-8585, Japan

Received 24 April 2002; received in revised form 10 December 2002

Abstract

We have carried out an experiment on the interaction between concentrated particles (hereafter called the Cluster) and Karman vortices in solid–liquid two-phase flow. The Karman vortices have been obtained by moving a cylinder in a shallow towing tank. The density of the particle is nearly the same as that of liquid. We have adopted High-resolution PIV to distinguish the Cluster velocity from the vector field of the surrounding flow. From the obtained data, we conclude that the Clusters enhance the steady rigid body rotation of the Karman vortices and the flow along the vortices. Furthermore, the Clusters keep their rotational motion and do not follow the flow along the vortices completely.

Keywords: Liquid–solid two-phase flow; Karman vortices; High-resolution PIV; Stokes number; Cluster; Rigid body rotation

1. Introduction

Interest has been growing in the interaction between particles and local flow structure in particulate two-phase flow, e.g., Kulick et al. (1998), Wang et al. (1998), Druzhinin (1994), Martin and Meiburg (1994) and Wang (1992). The particulate two-phase flow is encountered in pneumatic conveyance, fluidized bed, hydro-transport of solid particles in pipeline, and so on.

In the gas–solid two-phase flow, Tang et al. (1992) and Crowe et al. (1995) showed that the organization of particles around vortices in a bluff body wake depends on the Stokes number. The Stokes number is defined as $St = \tau_p/\tau_f$ where τ_p is the particle relaxation time and τ_f is the fluid

* Corresponding author. Tel.: +81-75-724-7324; fax: +81-75-724-7300.
E-mail address: yoshi@ipc.kit.ac.jp (Y. Hagiwara).

0301-9322/03/$ - see front matter
doi:10.1016/S0301-9322(02)00168-4

time. At the Stokes number of unity, the particles were focused into thin regions at the edge of the vortex structures, e.g., Wen et al. (1992) and Yang et al. (2000). At the Stokes number of 0.01, the particles followed the flow and filled in the vortex structures which were formed and convected downstream. τ_p was derived from the equation of motion for an isolated particle of any kind of material in a flow field. This equation is called Boussinesq–Basset–Oseen (BBO) equation. The equation, derived from fundamental principles by Maxey and Riley (1983), can be written for the case of low particle Reynolds number ($Re < 1$) as follows:

$$\left(1+\frac{1}{2}\frac{\rho_f}{\rho_p}\right)\frac{d\boldsymbol{u_p}}{dt}=\frac{3}{2}\frac{\rho_f}{\rho_p}\frac{D\boldsymbol{u_f}}{Dt}+\frac{18\mu}{\rho_p d_p^2}(\boldsymbol{u_f}-\boldsymbol{u_p})+\left(1-\frac{\rho_f}{\rho_p}\right)g + \frac{3}{\sqrt{2\pi}}\sqrt{\frac{\rho_f}{\rho_p}}\sqrt{\frac{18\mu}{\rho_p d_p^2}}\int_0^t\left(\left[\frac{D\boldsymbol{u_f}}{Dt}-\frac{d\boldsymbol{u_p}}{dt}\right]\Big/\sqrt{t-\tau}\right)d\tau, \quad (1)$$

where $\boldsymbol{u_f}$ is the velocity of the carrier fluid, $\boldsymbol{u_p}$ is the velocity of the particle, ρ_f is the fluid density and ρ_p is the particle density. This equation can be nondimensionalized by introducing a representative flow velocity, U_r, and a length scale L. For "heavy" particles, i.e. $\rho_f/\rho_p \ll 1$, the equation is reduced to:

$$\frac{d\boldsymbol{u_p}}{dt}=\frac{18\mu L}{U_r\rho_p d_p^2}(\boldsymbol{u_f}-\boldsymbol{u_p})+\frac{Lg}{U_r^2}. \quad (2)$$

This is the conventional equation used for predicting the motion of a particle in gas–solid two-phase flows. The coefficient of the first term in RHS was determined as the Stokes number by Tang et al. and Crowe et al.

However, the organization cannot be predicted with Eq. (2) for the case of motion of particles in liquids where $\rho_f/\rho_p \approx 1$. In this case, all the terms in the BBO equation must be retained. Thus, the equation for particle motion is much more complicated to solve.

As far as the present authors know, there are few experimental and numerical data on the organization for particles at the Stokes number of unity and vortices in liquid–solid two-phase flow. Tanaka et al. (2001) reported that the particles were focused into thin regions at the edges of vortex structures in liquid–solid two-phase flow.

In the present study, we carry out the experiments on the behavior of solid particles near Karman vortices in order to investigate the influence of the organization on the vortices. We focus particularly on the interaction between the Cluster and Karman vortices. This interaction is evaluated by statistical quantities associated with the Cluster area fraction and the rigid body rotation of the flow field.

2. Apparatus and experimental procedure

2.1. Apparatus

Fig. 1 shows a sketch of the apparatus. The support of a circular cylinder consisted of three parts: a bench, an arm and a finger. The bench was towed by a belt, which was moved by a motor

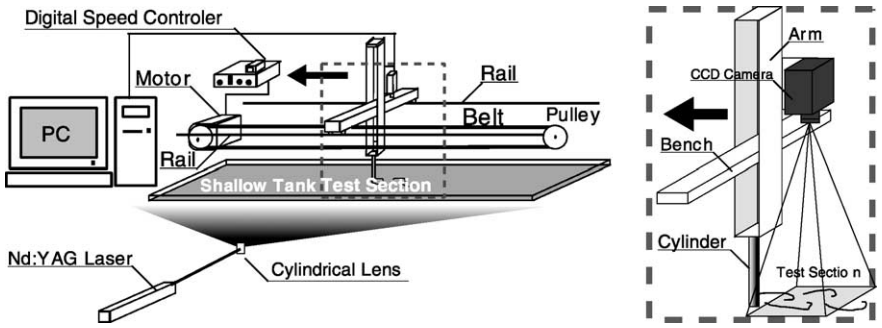

Fig. 1. The towing tank.

with a constant speed in a shallow water tank ($2.0 \times 0.25 \times 0.03$ m^3). The speed was controlled by a motor with a digital speed controller. The arm was fixed at the center of the bench and equipped with a CCD camera. The circular cylinder was fixed at the pointed end of the arm with a screw. The lowest part of the cylinder was immersed in water at the depth of 0.025 m. The clearance between the bottom of the cylinder and the bottom surface of the water tank was 2×10^{-4} m.

All the particles were scattered into the water before starting a series of experiments. The following procedures were carried out in each run in the experiment: (1) after all the particles became stationary, the cylinder was moved in one direction, (2) the cylinder was stopped moving after a certain period, (3) the cylinder was moved back to the original position.

2.2. Experimental condition

In this experiment, Karman vortices were measured as a two-dimensional flow on the free surface. The parameters for Karman vortices were $D = 0.015$ m for the diameter of the circular cylinder and $U_{\mathrm{cyl}} = 0.13$ m/s for the speed of moving cylinder. The water temperature was kept at 291 K. Experiments were conducted at a Reynolds number ($Re = U_{\mathrm{cyl}}D/\nu$) of 1.8×10^3, where ν is the kinematic viscosity ($\nu = 1.06 \times 10^{-6}$ m^2/s).

2.3. Image capturing and image processing

The measuring area was determined so that at least four vortices can be observed. The area was 0.143×0.108 m^2, located 0 m from the surface of circular cylinder. The successive images were captured by a progressive-scan CCD camera (SONY XC-8500: nominal frame rate; 50 frames/s at 760×572 pixels resolution) for 3 s (151 frames) in a series, and the images were stored in a personal computer. Ten series of images were captured in each case.

The light source was a green Nd:YAG laser (wavelength; 5.32×10^{-7} m, mode; PW, power; 3.8 W at 10 kHz). The laser light was expanded to a light sheet of 0.02 m in thickness. A mirror was allocated outside the other wall of tank to reflect the light sheet. The thick light sheet and the mirror are effective for illuminating all the particles mentioned below and obtaining sufficient intensity of fluorescence from the particles.

We made fluorescent tracer particles by coating polyethylene particles (Sumitomo Seika Chemicals Co., Ltd., Japan, FLO-THENE) with red florescent colour. The wavelength of fluorescence was approximately 6.0×10^{-7} m. We arranged a sharp-cut optical filter (Fuji Film, SC-56, wavelength threshold; 5.6×10^{-7} m) in front of the CCD camera in order to reduce the intensity of green laser light reflected by the tank and the cylinder.

The diameter of tracer particles was in the range of $1.0 \times 10^{-4} \leqslant d_p \leqslant 2.0 \times 10^{-4}$ m. We determined this range because we obtain enough intensity of fluorescence from the tracer particles. The density of the particles ρ_p was approximately equal to 9.5×10^2 kg/m^3. The acceleration of the particle by fluid flow was estimated by the following equation:

$$\frac{3}{2}\frac{\mathrm{d}u_p}{\mathrm{d}t} = \frac{3}{2}\frac{\mathrm{d}u_f}{\mathrm{d}t} + \frac{18v}{d_p^2}(u_f - u_p), \tag{3}$$

where u_p and u_f are the axial component of particle velocity and that of fluid velocity, respectively. This equation is derived from Eq. (1) with the assumptions of $\rho_p = \rho_f$, and the neglect of fluid convection terms and the last term in RHS of Eq. (1). Assuming that u_p is equal to zero at $t = 0$, u_p is obtained from Eq. (3) as follows:

$$u_p = u_f\left\{1 - \exp\left(-\frac{12v}{d_p^2}t\right)\right\}. \tag{4}$$

Thus, the moment t_p when u_p becomes equal to $0.99u_f$ and the particle traveling distance l_p for the period from 0 to t_p are as follows:

$$t_p = 0.38\frac{d_p^2}{v}, \quad l_p = u_f\left[t_p + \frac{d_p^2}{12v}\left\{\exp\left(-\frac{12v}{d_p^2}t_p\right) - 1\right\}\right]. \tag{5}$$

t_p was in the range of 0.0036–0.014 s. The highest value for l_p was evaluated by setting u_f equal to U_{cyl}, and was 0.0014 m. The upper limit of the frequency, beyond which u_p is lower than $0.99u_f$ in the case of flow with sinusoidal fluctuation, was estimated from the equation derived by Hjelmfelt Jr. and Mockros (1966). The frequency was approximately 70 Hz. This is higher than the frequency for the vortex street and the frame rate. Therefore, it is considered that the traceability of the red fluorescent particles is high enough.

High-resolution PIV with a gradient method (Sugii et al., 2000) was applied for the captured images. A hierarchical algorithm for grid refinement described in the following is included in this PIV:

Step 1: Calculate the cross-correlation.
Step 2: Remove erroneous vectors using a neural network and an interpolation with Laplace equation rearrangement (hereafter called LER) (Murai et al., 1998).
Step 3: Project the estimated displacement data onto the next higher resolution level. Use this displacement data to offset the interrogation windows with respect to each other.
Step 4: Increase the resolution level and repeat Steps 1 through 4 until the standard image resolution is obtained.
Step 5: Finally perform an interrogation at the desired interrogation window size and calculate sub-pixel displacement using the gradient method (without the neural network and LER).

We adopted the interrogation window of 32×32 pixels in the first stage, then that of 16×16 pixels in the second stage, and finally that of 8×8 pixels in the iterative procedure of Steps 1 through 4. The velocity vector field calculated by this High-resolution PIV is drawn with 174×127 grid points and four pixels grid spacing. The noise of obtained PIV data is removed by convoluting with a Gaussian filter ($\sigma = 1.0$, 5×5 pixels). The computational time was 6 h for 151 frames using a PC with CPU of Pentium III 866 MHz.

2.4. Particle condition

We made particles in the dispersed-phase (hereafter called Particle) by coating polystyrene particles with red fluorescent colour. The diameter of Particle was in the range of $1.1 \times 10^{-3} \leqslant d_p^* \leqslant 1.2 \times 10^{-3}$ m. The ratio of d_p^*/d_p was in the range of 5.5–12. The density of the Particle ρ_p^* was equal to 9.5×10^2 kg/m^3.

The brightness of the fluorescence from the Particle was higher than that from the tracer particles. Thus, the images of Particles can be distinguished from those of tracer particles. Note that the peak value of the brightness for the Particle is much lower than the product of 5.5^2 and the peak value of the brightness for the tracer particle. This shows that the intensity of fluorescence does not increase with the square of particle diameter. This is different from the intensity of scattered light from particles, which is approximately proportional to d_p^2 (Raffel et al., 1998). Therefore, the effect of fluorescence from a Particle on the images of tracer particles near the Particle is not serious. Actually, all the tracer particles were visible even very close to the Particles in some sampled images. The identical PIV was applied for all the particles including the clustering Particles.

2.5. Stokes number

Since there is no clear definition of the Stokes number for the case of $\rho_f/\rho_p \approx 1$, we defined the Stokes number for our experiment as follows:

$$St = \tau_p/\tau_f = \frac{(2\rho_p + \rho_f)}{36\mu} d_p^2 \Big/ \frac{D}{U_{cyl}}. \tag{6}$$

This equation is derived from Eq. (1) by nondimensionalizing with U_{cyl} and D, and dividing by $(1 + ((1/2)(\rho_f/\rho_p)))$. Note that we considered only the second term in RHS of the reduced Eq. (1). The Stokes number of the Particle was in the range of $0.80 \leqslant St^* \leqslant 0.95$.

The Stokes number of the tracer particle was in the range of $0.0066 \leqslant St \leqslant 0.026$. Judging from the results obtained by Wen et al. (1992) and Yang et al. (2000) mentioned in Section 1, the tracer particles followed the Karman vortices and filled in the vortex structure.

2.6. Particle area fraction

To investigate the influence of the interaction between the Particle and its surrounding flow on the whole flow field, we need to know the particle number density in the observation area. Since we dealt with the two-dimensional images, the particle area fraction, α, was considered for the number density. α was defined as the ratio of the area of the Particle existing in the observed flow

Table 1
Observed value of the particle area fraction

α (%)	Observed value ($\bar{\alpha}$%)
5	4.9 ± 0.4
10	9.3 ± 2.5
15	13.4 ± 2.7

Here, $\bar{\alpha}$% is the average of 10 samples in each α, and $\pm$ denotes its standard deviation.

field to that of the observed flow field. The area of the Particle was determined as the region where the brightness was above a threshold in the digital image.

In order to measure the particle area fraction quantitatively, we made a tray having 5% of the area of the water tank. We laid the Particle in the tray without space, and we can measure the particle area fraction at 5% quantitatively.

For evaluating this method, the particle area fraction is calculated with images of 1500 frames each in the particle area fractions. The evaluated results are shown in Table 1.

3. Results and discussion

A local concentration of the Particle increases with the number of Particles in the flow field. We investigated the interaction between the Cluster and large scale vortices in this study. We focused on the large scales for the Cluster in space and time. We also observed the influence of the Cluster on the vorticity as the rigid body rotation in the following subsections.

3.1. Definition of Cluster

The definition of the Cluster differs according to each researcher, e.g., Yonemura et al. (1995) and Horio and Ito (1997). We define a Particle which satisfied the following two conditions as the Cluster.

1. Existing in the area of shedding vortices behind the cylinder.
2. Nearly contacting to another Particle.

The area, S_v is defined as the area where the frequency is the range of 1.8–1.9 Hz, which is nearly the same as the frequency of shedding vortices (1.9 Hz, Roshko, 1953). Here, the frequency was obtained from time-varying velocity at each grid point with FFT. The gray area in Fig. 2(a) shows an example of the area. Karman vortices flowed from right to left in this figure. The white areas in Fig. 2(b) indicate the Particles. Some of the areas, which fulfill the condition 1, are considered as the candidate of the Clusters. Fig. 3(a) depicts the candidates. Some of the candidates, which fulfill the condition 2, are considered as the Clusters. All the areas inside the rectangle drawn in Fig. 3(a) are the Clusters. Fig. 3(b) indicates the velocity vectors inside the rectangle. The grid space (four pixels) is smaller than the diameter of the Particle (12 pixels) in the Clusters. Therefore,

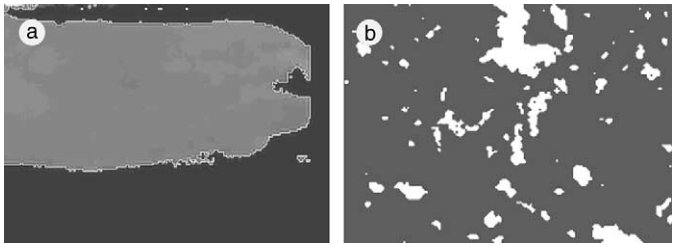

Fig. 2. Area of shedding vortices and Particle distribution. (a) Area of shedding vortices, (b) distribution of particles ($\alpha = 15\%$).

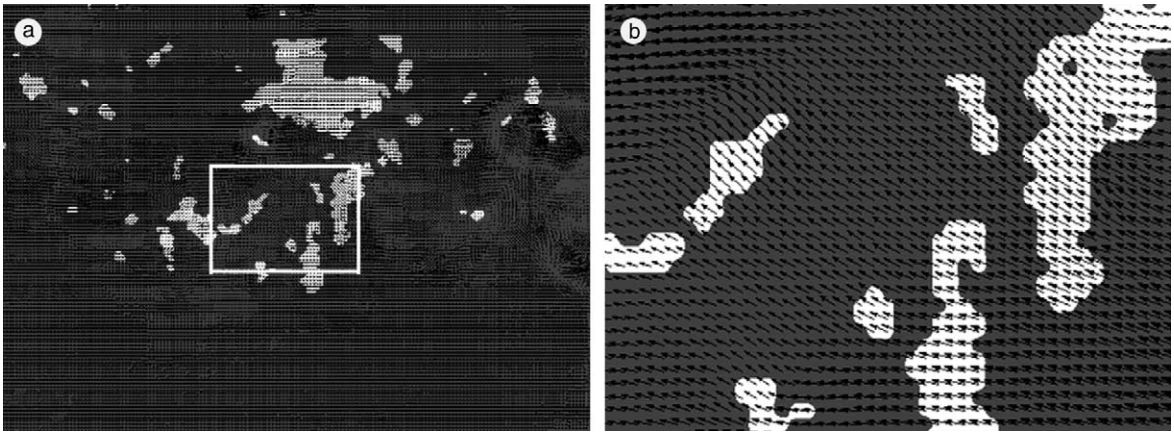

Fig. 3. Cluster and velocity. (a) Cluster ($\alpha = 15\%$), (b) Magnified image of Cluster ($\alpha = 15\%$).

nearly contacting Particles inside the Clusters are found to have a nearly identical velocity. We consider the velocity as the Cluster velocity.

3.2. Spatial and time scales of Cluster

Tang et al. (1992) reported the self-organization of particles, which was characterized as the relation between large-scale particle dispersion and small-scale particle dispersion using the correlation dimension. However, the correlation dimension could not be observed from the spatial and time development of the Cluster. We introduce the Cluster area fraction, $\alpha_C(t)$, to observe the spatial and time development of the Cluster. $\alpha_C(t)$ was defined as the ratio of the area of the Cluster to S_v at any moment.

The time average of the Cluster area fraction, $\overline{\alpha_C}$, was calculated from $\alpha_C(t)$. $\overline{\alpha_C}$ is plotted as a function of α in Fig. 4. The vertical lines in this figure indicate the range for the fluctuation of $\overline{\alpha_C}$. This figure shows that $\overline{\alpha_C}$ increases with α. This relation means that the spatial scale of the Cluster in the area of shedding vortices becomes larger than the dispersed Particle (not clustering Particle) in the area.

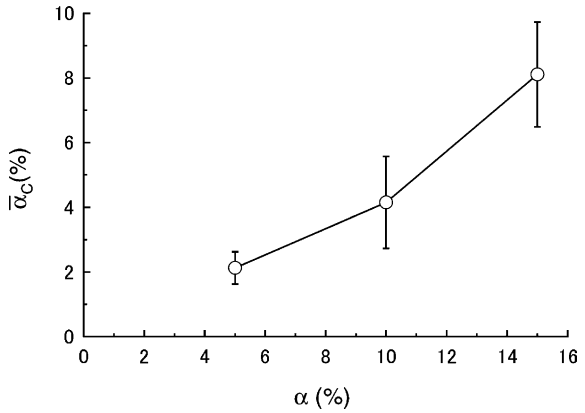

Fig. 4. Cluster area fraction.

The power spectrum for the Cluster area function, $|\alpha_C(\omega)|^2$, was obtained from the spatial mean value of $\alpha_C(t)$ with FFT. Fig. 5 shows the power spectra. In each case of α, the spectrum has a peak at the low frequency, which is lower than the frequency of shedding vortices (1.9 Hz). This frequency is related to the Clusters transported by meandering flow caused by the Karman vortices. The peak value decreases with an increase in α. This indicates that the Clusters, particularly the large-scale Clusters have different motion from fluid motion in the meandering flow.

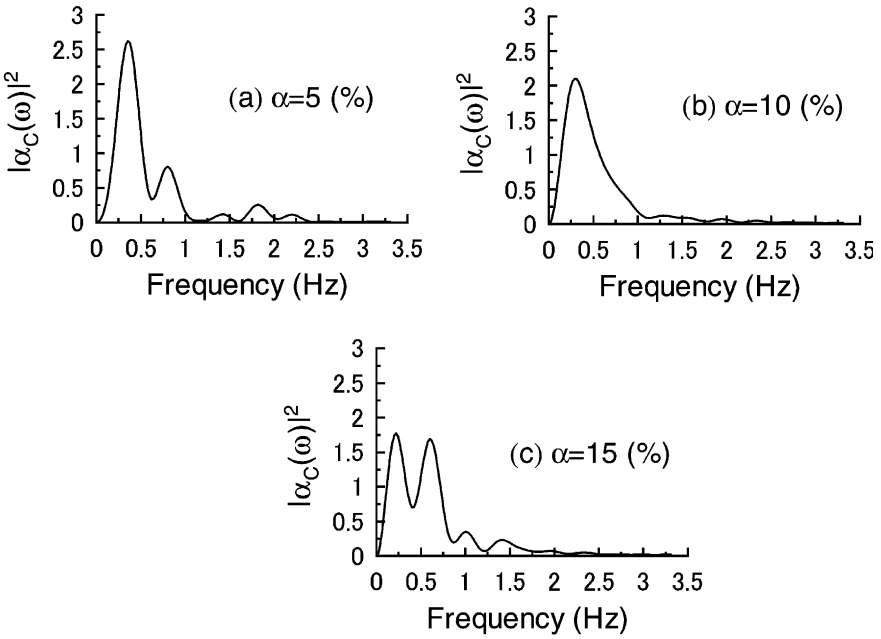

Fig. 5. Power spectra of Cluster area fraction.

3.3. Rigid body rotation enhanced by the Cluster

From these results, we consider that the development of the Cluster enhances the rigid body rotation in the Karman vortices. To confirm this enhancement, we investigate the influence of the Cluster on the rigid body rotation defined as follows:

$$R(t) = \int_{S_v} \left| \frac{\partial u_x(x,y,t)}{\partial y} - \frac{\partial u_y(x,y,t)}{\partial x} \right| \mathrm{d}s = \int_{S_v} |\Omega| \mathrm{d}s, \tag{7}$$

where u_x and u_y are the velocity in the axial direction and that normal to the axis, respectively, and Ω is the vorticity. Then, $R(t)$ is nondimensionalized with U_{cyl} and D. The time-averaged value of the nondimensionalized rotation, $\overline{R^+}$, is plotted as a function of the particle area fraction in Fig. 6. The vertical lines in this figure indicate the range for the fluctuation of $R(t)$. This figure shows that $\overline{R^+}$ increases with α, which is similar to the result showing that $\overline{\alpha_C}$ increases with α as shown in Fig. 4.

We obtained the power spectrum of the rigid body rotation, $|R^+(\omega)|^2$, by applying FFT to $R(t)$. Fig. 7 shows the power spectra. The maximum of the spectrum at around 0.3 Hz is associated with the meandering flow induced by the Karman vortices. This maximum value increases with α. The peak of the spectrum at around 1.9 Hz is associated with the vortex shedding. This peak value also increases with α.

These results indicate that the Cluster enhances the rigid body rotation. By considering a decrease in the kinetic energy of flow with an increase of α or α_C (Tanaka et al., 2001; Tanaka, 2002), it is concluded that kinetic energy was transferred from the flow to the Clusters and used for the enhancement of rigid body rotation in the flow.

3.4. Interaction between the Cluster and the rigid body rotation

In order to observe the interaction between the Cluster and the rigid body rotation directly, we pay attention to the time change in $\alpha_C(t)$ and $R^+(t)$ in the case of $\alpha = 15\%$. Figs. 8 and 9 show the typical time series of $\alpha_C(t)$ and $R^+(t)$, respectively. It is observed for the period drawn by the bold

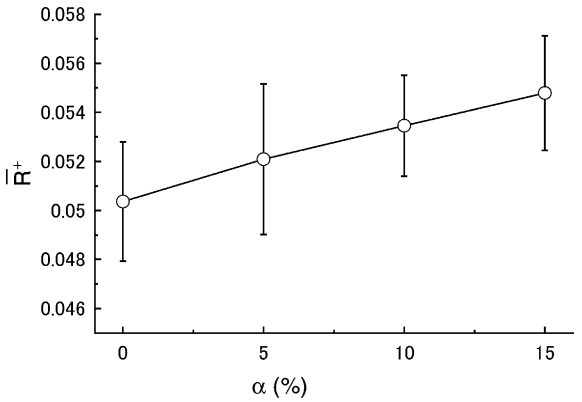

Fig. 6. Rigid body rotation.

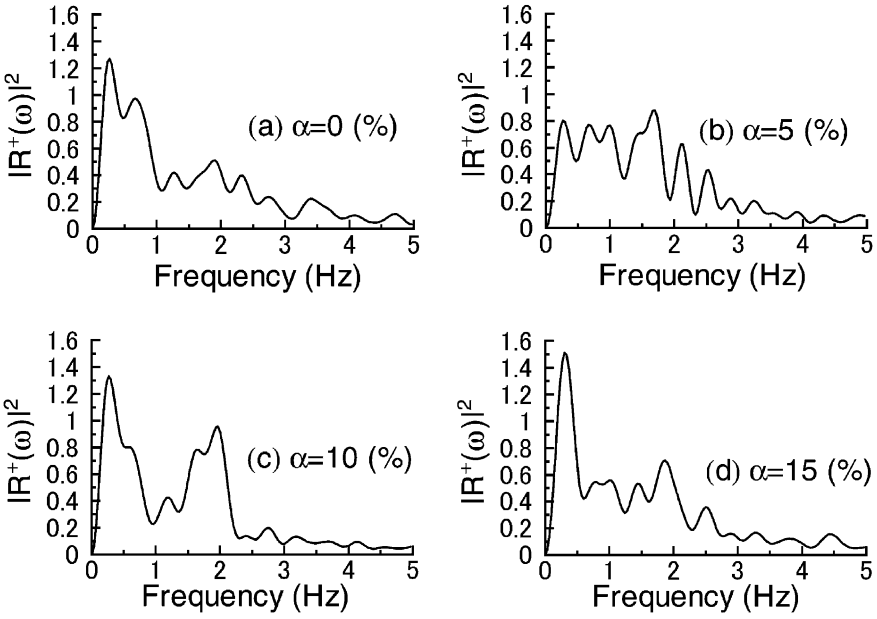

Fig. 7. Power spectra of rigid body rotation.

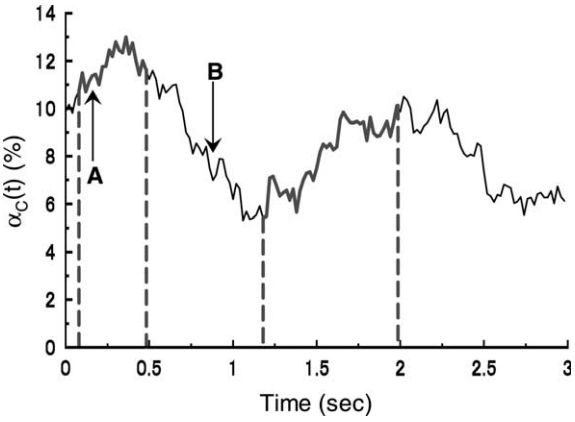

Fig. 8. Cluster area fraction ($\alpha = 15\%$).

lines that the increase of $\alpha_C(t)$ with time brings about the stabilizing of $R^+(t)$. We observed the organization of the Cluster shown in Fig. 10(a) at the instant **A** in the first period in Figs. 8 and 9. Note that the Clusters in Fig. 10(a) are concentrated around the edges of the vortices, which is in agreement with the results obtained by Tang et al. (1992) and Crowe et al. (1995) mentioned above. On the other hand, the decreasing of $\alpha_C(t)$ brings about the fluctuation of $R^+(t)$. We did not observe the organization of the Cluster in Fig. 10(b) at the instant **B** shown in Figs. 8 and 9. Thus, we found that the organization of the Cluster plays an important role in this stabilizing of $R^+(t)$.

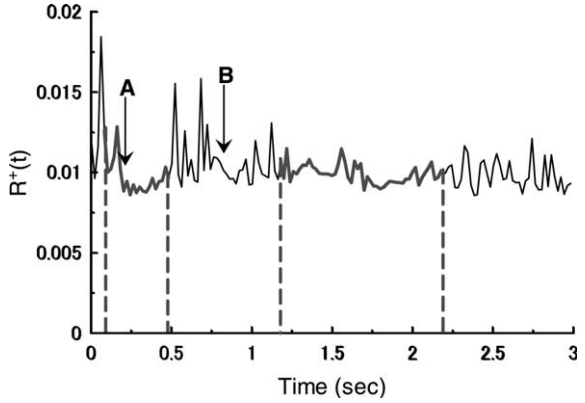

Fig. 9. Rigid body rotation $R^+(t)$ ($\alpha = 15\%$).

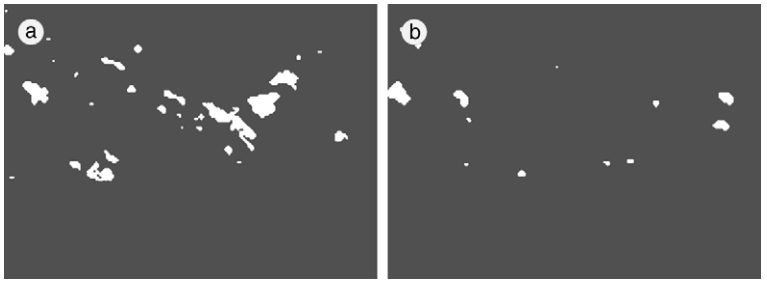

Fig. 10. Organization of Cluster. (a) Cluster ($t = 0.2$ s), (b) Cluster ($t = 0.8$ s).

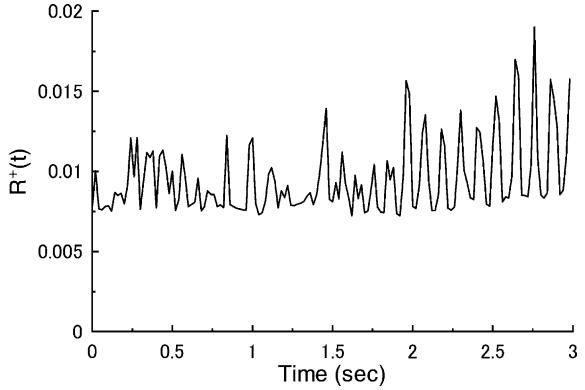

Fig. 11. Rigid body rotation $R^+(t)$ ($\alpha = 0\%$).

Fig. 11 shows the time series of $R^+(t)$ in the case without Particle. It is found by comparing Fig. 9 with Fig. 11 that the fluctuation of $R^+(t)$ ($\alpha = 15\%$) is less noticeable than that of $R^+(t)$ ($\alpha = 0\%$). The time-averaged value of $R^+(t)$ in Fig. 9 is 3% larger than that in Fig. 11. This indicates that the rigid body rotation of the Cluster attenuates the fluctuation of $R^+(t)$. It is

concluded from these results that the Clusters concentrated along the edge of the vortices enhance the stable rigid body rotation and the meandering flow along the vortices. Since the Clusters keep their rotational motion, the Clusters do not follow the meandering flow completely.

4. Conclusion

We carried out the experiment on the interaction between Karman vortices and particles in a solid–liquid two-phase flow. The main conclusions obtained are as follows:

1. The Clusters, which are concentrated along the edge of the Karman vortices, enhance the stable rigid body rotation of the vortices and the meandering flow along the vortices.
2. The Clusters do not follow the meandering flow completely because they keep their rotational motion by using the kinetic energy from the fluid flow.
3. The velocity field was divided into the Cluster and the surrounding flow using High-resolution PIV.

Acknowledgements

The authors wish to thank Mr. Kawasaki (technical staff) for support in producing experimental apparatus.

References

Crowe, C.T., Troutt, T.T., Chung, J.N., 1995. Particle interactions with vortices. In: Green, S.I. (Ed.), Fluid Vortices. Kluwer Academic Publishers, pp. 829–861.

Druzhinin, O.A., 1994. Concentration waves and flow modification in a particle-laden circular vortex. Phys. Fluids 6, 3276–3284.

Hjelmfelt Jr. A.T., Mockros, L.F., 1966. Motion of discrete particles in a turbulent fluid. Appl. Sci. Res. 16, 149–161.

Horio, M., Ito, M., 1997. Pediction of cluster size in circulating fluidized beds. J. Chem. Eng. Jpn. 30, 691–697.

Kulick, J.D., Fessler, J.R., Eaton, J.K., 1998. Particle response and turbulence modification in fully developed channel flow. J. Fluid. Mech. 277, 109–134.

Martin, J.E., Meiburg, E., 1994. The accumulation and dispersion of heavy particles in forced two-dimensional mixing layer. I. The fundamental and subharmonic cases. Phys. Fluids 6, 1116–1131.

Maxey, M.R., Riley, J.J., 1983. Equation of motion for a small rigid sphere in a nonuniform flow. Phys. Fluids 26, 883–888.

Murai, Y., Ido, T., Ishikawa, M., Yamamoto, F., 1998. Development of post-processing method for PIV measurement result using computational fluid dynamics procedure. Trans. Jpn. Soc. Mech. Eng. (B) 64, 3249–3256 (in Japanese).

Raffel, M., Willert, C., Kompenhans, J., 1998. Particle Image Velocimetry A Practical Guide. Springer-Verlag, Berlin, p. 17.

Roshko, A., 1953. On the development of turbulent wakes from vortex streets. NACA Technical Note 2913.

Sugii, Y., Okuno, T., Nishino, S., 2000. High-resolution adaptive PIV technique using gradient method. In: 9th International Symposium on Flow Visualization, Heriot-Watt University, Edinburgh 2000, p. 337 (on CD-ROM).

Tanaka, Y., 2002. M.Sc. Thesis of Kyoto Institute of Technology.

Tanaka, Y., Hagiwara, Y., Tanaka, M., Murata, T., 2001. Diameter dependence of the motion of solid particles near vortices in liquid flow. PSFVIP-3 Maui, Hawaii 18–21 March 2001, F3407, pp. 1–11 (on CD-ROM).

Tang, L., Wen, F., Yang, Y., Crowe, C.T., Chung, J.N., Troutt, T.T., 1992. Self-organizing Particle dispersion mechanism in a plane wake. Phys. Fluids A 4, 2244–2251.

Wang, L.P., 1992. Dispersion of particles injected nonuniformly in a mixing layer. Phys. Fluids A 4, 1599–1601.

Wang, Q., Squires, K.D., Wang, L.P., 1998. On the effect of nonuniform seeding on particle dispersion in two-dimensional mixing layers. Phys. Fluids 10, 1700–1714.

Wen, F., Kamalu, N., Chung, J.N., Crowe, C.T., Troutt, T.R., 1992. Particle dispersion by vortex structures in plane mixing layers. J. Fluids Eng. 114, 657–666.

Yang, Y., Crowe, C.T., Chung, J.N., Troutt, T.R., 2000. Experiments on particle dispersion in a plane wake. Int. J. Multiphase Flow 26, 1583–1607.

Yonemura, S., Tanaka, T., Tsuji, Y., 1995. Numerical simulation of cluster formation in gas–solid flow (effects of particle size and particle concentration on the structure of clusters). Trans. Jpn. Soc. Mech. Eng. (B) 61, 3671–3678 (in Japanese).